

## STUDY OF RELATIVISTIC ENERGY $^{207}\text{Pb}$ PROJECTILE FRAGMENTATION ON HEAVY TARGETS

\*G. SHER, M.I. SHAHZAD, S. MANZOOR, M.A. RANA and Z. YASIN

Physics Division, Directorate of Science, PINSTECH, P.O. Nilore, Islamabad, Pakistan

(Received June 07, 2010 and accepted in revised form August 17, 2010)

---

Fragmentation of 158 A GeV  $^{207}\text{Pb}$  projectiles is studied on Bi, Pb, Cu and Al targets using CR-39 nuclear track detectors. Stacks containing detectors and targets were exposed at SPS beam facility of CERN. After chemically etching, detectors were scanned with an optical microscope. Lengths of etched cones produced as a result of beam ions and the fragments in the detectors have been measured. The charge resolution ( $\sigma_Z$ ) achieved by this technique in the charge region  $63 \leq Z \leq 82$  is  $\sim 0.3e - 0.2e$ . The total charge-changing cross sections have been determined using the statistics of etched cone heights corresponding to the projectile ions and their nuclear fragments. Measured total charge-changing cross sections are compared to the corresponding calculations with semi-empirical models and predictions of the FLUKA code. The dependence of total cross sections on the projectile and target mass is also described.

**Keywords:** Relativistic energy, Pb projectiles, Fragmentation, Cross sections, CR-39 detectors

---

### 1. Introduction

Projectile fragmentation studies can provide information about the fragmentation mechanism and liquid-gas phase transition process in hot nuclei and help to trace the reaction mechanism of nucleus-nucleus collisions. In these experiments the main interest is focused on nucleon-nucleon interaction with small impact parameters corresponding to the significant overlap of nuclei. Central collisions are most appropriate for studying the highly excited and compressed hadronic matter and quark gluon plasma [1]. Peripheral collisions are used to study the fragmentation of spectators. However, the collisions with impact parameters exceeding the sum of nuclear radii, i.e., with no direct overlap of nuclei, can also significantly contribute to the nuclear reactions via the long-range electromagnetic interaction. At relatively non central impact parameter of interacting nuclei, reactions are exhibited eventually giving rise to the fragmentation of the excited nuclei leading to the emission of fragments with a wide mass spectrum. The fragmentation charge changing cross sections are important to estimate the composition of the cosmic rays and their propagation through the interstellar medium [2].

Several authors have investigated projectile fragmentation at relativistic energies on different projectile-target combination using active as well as passive (SSNTDs) detection techniques and measurement of total and partial charge changing cross sections have been reported [3-8].

FLUKA is a Monte Carlo simulation package, written in Fortran language, for a variety of models of particle transport and interaction with matter [9,10]. The FLUKA program is one of the most useful simulation tools for many applications in high-energy physics and engineering. FLUKA can simulate the interaction and propagation in matter of more than 60 different particles (in practice, FLUKA considers all particles listed in the Particle Data Book [10-11], except for hadrons with bottom and heavier quarks)—such as heavy-ions, electrons, neutrons, photons, neutrinos and muons—in many types of research fields: shielding design, detector response studies, cosmic-ray studies, medical physics, and dosimetry calculations. In recent years FLUKA has been extensively developed and improved, the newest version introducing many fundamental changes to the implementation of modern physics algorithms, as well as programming upgrades.

---

\* Corresponding author : gsher@pinstech.org.pk

We have used CR-39 nuclear track detectors in this experiment manufactured by Intercast Europe Co. Parma, Italy. The response of this detector towards a wide range of projectile charge and energies has been extensively recognized in various experimental studies [12-19]. We report in section 2, the experimental technique, results are discussed and compared with FLUKA calculations in section 4 and section 5 contains the conclusions.

## 2. Experimental Procedure

For this experiment four stacks containing Bi, Pb, Cu and Al targets sandwiched with several CR-39 nuclear track detectors of size (11.5cm x 11.5cm x 1mm) were exposed to the 158 A GeV Pb ions at the SPS heavy ion beam of CERN. The exposure of each stack was performed at normal incidence. The total number of lead ions in each stack was about  $7.8 \times 10^4$ , distributed in eight spots. The central density in each spot was about  $1500 \text{ ions/cm}^2$ .

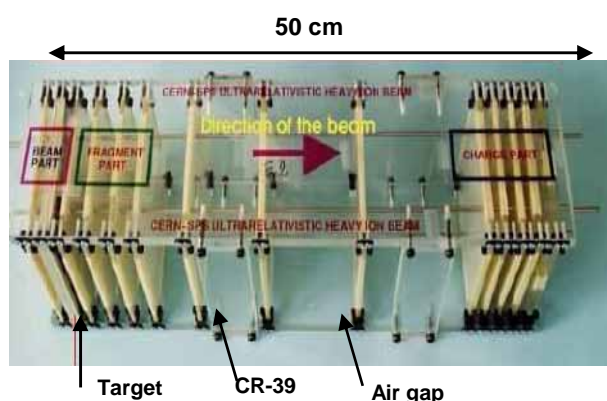


Figure 1. Sketch of the target-detector configuration used for the exposures. For the present study, one detector upstream of the target and another downstream of the target were used for etching and the follow-up nuclear track measurements in all four target-detector stacks.

For the exposure of stacks containing targets and detectors we used the geometry sketched in Fig. 1. Four CR-39 detector sheets were placed upstream and more than 40 detectors downstream of the target in the exposure stacks. We have selected one CR-39 detector upstream and another detector downstream of the targets from each stack and etched in 4N KOH aqueous solution at  $45^{\circ} \text{C}$  for 72h in a thermostat etching bath provided with continuous stirring. The KOH etchant has been selected due to its very small swelling effect on CR-39 sheets. After etching, the

beam ions and the fragments registered in the CR-39 detectors appeared as cylindrical cones on both sides of the CR-39 detector.

The diameters of the etched cones have been measured by an optical microscope with a filar micrometer eye piece and the lengths with Heidenhain depth measuring linear transducer attached with the stage of the optical microscope. The smallest value of measurements was  $1 \mu\text{m}$ .

We have used a tracking procedure for the reconstruction of tracks produced in the first detector and in the second detector surface down stream of the targets. The average track lengths have been computed for each etched cone on two surfaces of the detectors. Figure 2(a, b) shows the average cone height distributions for 158A GeV Pb beam ions registered in the detector placed before and their fragments registered after the target.

CR-39 detectors, placed upstream of the targets registered the total number of incident Pb ions and detectors placed after the target recorded both the surviving Pb ions and the fragments produced in the interaction of the Pb ions with the targets. The bulk etch velocity  $v_B$  of the detector was measured by the change in the thickness of the detector before and after etching of the detector. For this etching time, the change in the detector thickness is measured and the average bulk etch rate  $v_B$  was  $v_B = 0.140 \pm 0.012 \mu\text{m/hr}$ . The refractive index of the CR-39 has been found to be 1.561, by measuring the actual thickness of the detector by depth measuring instrument and observed thickness using an optical microscope. The measured cone length has been multiplied with the calculated refractive index to determine actual etched cone height. The detectors upstream the target and the other downstream of the target from each target detector combination stack have been etched and scanned for the measurement of etched cones parameters using an optical microscope.

The ionizing particles passing through an insulating material create a narrow path of intense damage on an atomic scale [14]. The damaged region in the detector can be revealed and enlarged by treating with a proper chemical reagent to become visible under an optical microscope. The etch pits of conical shape are formed during the etching along the particle tracks on the surface of detectors. The size of the etch pits along the

track increases with the ionization energy loss, i.e. with charge for the relativistic ions. The focused surface of the opening of the etch-pits looks like a dark, circular of well defined diameter. The undamaged region of the detector is etched with a constant velocity  $v_B$  and the damaged region with a velocity  $v_T$ . If  $v_T > v_B$ , a conical etch-pit is produced at the point of entrance and exit of the particle. The nuclear tracks in shape of the etched cone are formed on both surfaces of the detector sheets. The ratio  $p = v_T / v_B$  is an increasing function of  $Z/\beta$ , depends on diameter and length of the etch-pit. During the etching process etch pits of conical shape area are formed along the particle track on the surface of detectors. The size of these etch pits along the track increases with the ionization energy loss, e.g., for relativistic particles with their charge. The position and size of the mouth of all etch cones on all detector sides can be measured with an optical microscope. In the track etch detectors, the projectile and fragments with energy loss exceeding the threshold of the detector are registered. Therefore, for an ion with  $Z/\beta$  greater than the detector threshold ( $Z \sim 7e$  for Intercast CR-39), the etching process leads to formation of etched cone on each side of a detector along the ion path [13-15]. Since the beam ions exposure have been performed at normal incidence to the detector surface, the projectile ions and the fragments produced as a result of fragmentation almost maintain their longitudinal velocity along the direction of beam ions, and can easily be identified as a sequence of etch cones produced on the subsequent detector surfaces. Target fragments can be separated on the basis of their short range.

### 3. Charge Resolution and Calibration of Detectors

The size of the etch cone depends on the radiation damage which is proportional to the energy loss of the impinging ion. The momentum transfer in a relativistic nuclear collision is very small in comparison to the momentum of projectile, therefore projectile fragments emerge from collision into a narrow cone in forward direction having exactly the same velocity of the incident ions. Based on our experimental technique projectile and the fragments with charge greater than the detection threshold of the CR-39 are registered.

The etch cones of normally incident beam particles and their fragments are of circular shape

and completely black in direct illumination. After etching, some track structures are visible on the detector. These background objects are shallow and appear as black circular objects with a brighter centre. They are very similar to over etched tracks of stopping particles but their abundance excludes that they are particle tracks. Additionally we see tracks of target fragments, which have no preferred angular direction with short range due to the low energies. The central brightness can be used to separate particle tracks from background.

In the projectile fragmentation relativistic velocity fragments are emitted in a narrow forward cone. The distribution of fragments of accurately known  $Z/\beta$  can easily be resolved on a detector surface. For each stack we scanned the central region of the top sheet with an optical microscope with built in depth measuring unit and measured the length and diameters of more than 6500 beam particles, selecting only those in a narrow range of diameters so as to eliminate background fragments with different charge or velocity from the beam. With the coordinates of the projectiles in the top sheet as an input to the microscope stage control, the tracks of the surviving beam particles appeared at the expected positions (at these energies Coulomb scattering is negligible in plastic detectors) and the tracks of projectile fragments.

We show in Fig. 2 (a,b) the spectrum of the average cone height distribution of projectile and the fragments produced on the projectile fragmentation with the target.

The cone height peaks are assigned a charge value starting from  $Z = 82$  the main peak due to beam ions. One can see that all fragments with charge  $63 \leq Z \leq 82$  can be well resolved and separated.

At relativistic energies the energy loss of the ions traversing the detector material depends only on charge  $Z$ , therefore peaks of measured etched cone heights correspond to different charges. The fragments charge can be represented by assigning charge values to these peaks. This method is applicable as long as the projectile peak and the fragment peaks are clearly separated. However, with increasing area charge resolution deteriorate as the difference between adjacent peaks decreases. It has been reported by [15] that etched cones base area is sensitive to low  $Z$  charge

fragments, the cone height is practical for the charge resolution of fragments of high Z.

$$\sigma_Z = (\sigma_L) / (\delta_L / \delta_Z) \quad (1)$$

where  $\sigma_L$  is the standard deviation of the individual peaks assigned to charge values given in Table 1. The ratio  $\delta_L/\delta_Z$  is the slope of the plot of Z verses L as shown in Fig. 3. The charge resolution  $\sigma_Z$  on single surface of the detector in the charge region  $63 \leq Z \leq 82$  has been obtained to be  $0.3e-0.2e$ .

Table 1. Mean cone heights corresponding to various peaks in Fig. 1 alongwith the full width half maxima of fitted Gaussians on these histogram peaks, for the interaction of (158 A GeV) Pb ions with the Al target. Assigned charges and their resolution values are also given.

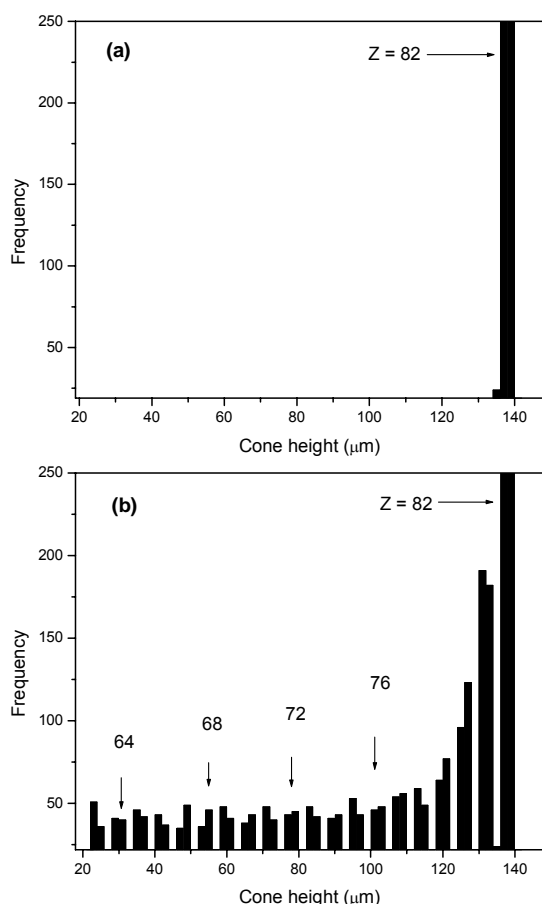


Figure 2. (a) shows the track length distribution of the incident beam of 158 A GeV Pb ions and (b) the fragments produced as a result of Pb ions interaction with Al target (as an example) recorded in the detector placed (a) upstream and (b) downstream of the targets. The arrows show the charge assigned to prominent peak is due to incident Pb projectile and the small peaks represent the projectile fragments.

We have therefore used the measured cone heights for the charge resolution of high Z projectile and fragments. The fragment with charges  $63 \leq Z \leq 81$ , having well separated peaks are assigned charge values by counting charge numbers downward beginning with the beam peak  $Z = 82$ . The peak at  $Z = 83$  corresponds to a charge pick-up reaction.

The charges assigned to each peak and charge resolutions in charge region  $63 \leq Z \leq 82$  are given in Table 1. The charge resolution is related to cone height resolution. The relative charge resolution is equal to the relative length resolution as follows

Charge (Ze)	Cone Length (μm)	Charge Resolution (e)
63	$23 \pm 1.1$	0.29
64	$29 \pm 1.1$	0.27
65	$35 \pm 1.1$	0.28
66	$41 \pm 1.0$	0.24
67	$47 \pm 1.0$	0.26
68	$53 \pm 1.1$	0.27
69	$59 \pm 0.9$	0.23
70	$65 \pm 1.0$	0.25
71	$71 \pm 0.9$	0.22
72	$77 \pm 1.0$	0.26
73	$83 \pm 0.9$	0.23
74	$89 \pm 1.0$	0.26
75	$95 \pm 1.0$	0.25
76	$101 \pm 0.8$	0.21
77	$107 \pm 1.1$	0.28
78	$113 \pm 1.0$	0.24
79	$119 \pm 1.0$	0.25
80	$125 \pm 1.1$	0.27
81	$131 \pm 0.9$	0.23
82	$137 \pm 0.8$	0.20

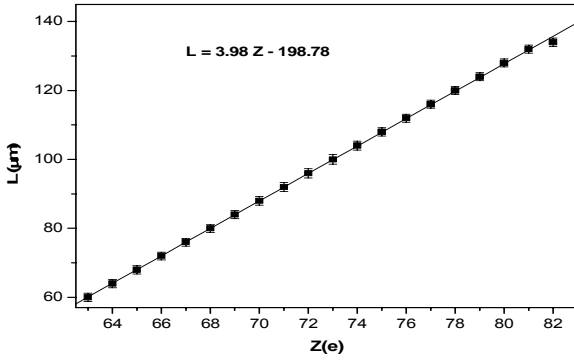


Figure 3. Correlation plot of the charges to their mean etched track lengths measured for detector placed after the target.

The detectors response to relativistic ions is characterized by the relation of the parameter  $p$  ( $v_T / v_B$ ), and restricted energy loss ( $REL$ ) from the calibration curve. Since the track etch rate  $v_T$  is a function of restricted energy loss ( $REL$ ) and  $REL$  is function of charge and energy of the incident charged particle, and for relativistic energy ions the  $REL$  remains approximately constant therefore, it may be considered that the diameter and length of etched cone are function of only charge  $Z$  [16]. At any given time of etching which is much less than the time required for revealing full track, the difference of  $v_T$  and  $v_B$  leads to the formation of a cone with a circular base of diameter  $D$  and cone length  $L$ . These two geometrical parameters are measured by using appropriate hardware attachments to an optical microscope. For normal incident particles,  $D$  is the surface etch-pit diameter. Previous calibrations had shown that the reduced etch rate  $p$  is a function of Restricted Energy Loss ( $REL$ ) only [14,27]. It is defined as that part of energy loss including only ionization in which  $\delta$  electrons with energy below threshold  $w_0$  are generated. For each detected charge the  $REL$  was computed using the Bethe-Bloch formula. The track diameters were obtained from the etch-pit surface area measurements.

The parameters  $D$  and  $L$  are related to ' $p$ ' through the equations [17]

$$D = 2 v_B t \sqrt{\frac{p-1}{p+1}} \quad (2)$$

$$L = v_B t (p-1) \quad (3)$$

where ' $t$ ' is the etching time.

The track etch rate  $v_T$  for the fragments produced in the interaction of 158 A GeV Pb ions with target using CR-39 is calculated from the relation,

$$v_T = v_B + \frac{L}{t} \quad (4)$$

The value of  $v_B$ , the bulk etch rate of the detector can be calculated by the change in the thickness of the detector before and after etching

$$v_B = \frac{\Delta X}{2t} \quad (5)$$

The bulk etch rate  $v_B$  has been determined to be  $0.140 \pm 0.012 \mu\text{m/h}$ . For the resolution of high  $Z$  fragment, we have used the method to associate different charges with cone heights. Further the charge values of fragments with almost identical  $\beta$  are associated with specific  $REL$  values while the lengths are converted to ' $p$ ' values through Eqn. 4. The  $REL$  vs.  $p$  graph as shown in Fig.4 constitute a calibration curve.

The values of restricted energy loss ( $REL$ ) are determined from the following expression.

$$REL = (dE/dx)_{E < E_{max} = 200\text{eV}} = C_1 \left(\frac{z}{\beta}\right)^2 \frac{Z_T}{A_T} \left[ \ln\left(\frac{C_2}{1}\right) - \frac{\beta^2}{2} - \frac{\delta}{2} \right] \quad (6)$$

where  $C_1 = 4\pi N_a r_e^2 m_e c^2$  and

$$C_2 = \sqrt{2 m_e c^2 \beta^2 \gamma^2 E_{max}}$$

At these energies the nuclear component of the energy loss is negligible. In Eqn. 6, the value of  $C_1 = 0.307 \text{ MeV.cm}^2.\text{g}^{-1}$ ;  $z/\beta$  refers to the ion fragment,  $Z_T$  and  $A_T$  are the average charge and mass values of the target (CR-39:  $Z_T/A_T = 0.533$ ), the mean ionization potential of CR-39 is  $I = 70\text{eV}$ ,  $E_{max} = 200\text{eV}$  [18] the density correction ' $\delta$ ' depends on the composition and state of the medium [28]. If the  $REL$  of a particle passing through a stack of foils is constant along its trajectory and the same etching conditions are applied to all the sheets of one stack, the *track etching rate*  $v_T$  is constant and identical cones are formed on all crossed detector surfaces.

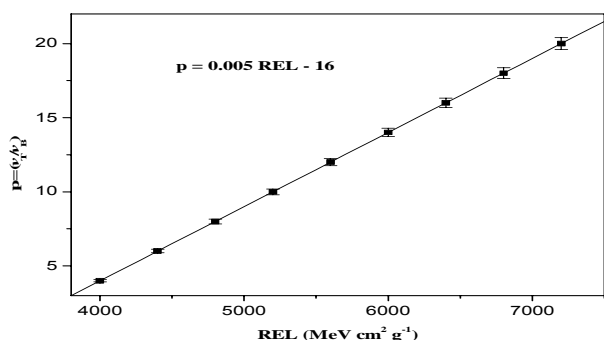


Figure 4. Calibration curve of reduced etch rate  $p$  vs  $REL$ . The points are the experimental data and the line is the best fit to the data point. The fitted equation is only valid in the  $REL$  range  $\sim 4000$ - $7100$  MeV cm<sup>2</sup>/g. The main contribution to the errors comes from the uncertainty in the determination of  $v_B$ . The uncertainties in the bulk velocity yield a systematic error on the reduced etch rate  $p$ .

### 3.1 Physics Models of FLUKA

A description of the intermediate and high energy hadronic interaction models used in the FLUKA code and benchmarking against experimental data are reported [9] in order to validate the model performance. Finally the most recent developments and perspectives for nucleus–nucleus interactions are described together with some comparisons with experimental data. FLUKA [9-11] is a multipurpose transport Monte Carlo code, able to treat hadron–hadron, hadron–nucleus, neutrino, electromagnetic, and  $\mu$  interactions up to 10000 TeV. Charged particle transport (handled in magnetic field too) includes all relevant processes [9]. About nucleus–nucleus collisions, since ion–ion nuclear interactions were not yet treated in FLUKA, past results have been obtained in the superposition model approximation, where primary nuclei (0–10000 TeV/A) were split into nucleons before interacting. Due to this “microscopic” approach to hadronic interaction modelling, each step is self–consistent and has solid physical bases. Performances are optimized comparing with particle production data at single interaction level. No tuning whatsoever is performed on “integral” data, such as calorimeter resolutions, thick target yields, etc. Therefore, final predictions are obtained with a minimal set of free parameters, fixed for all energies and target/projectile combinations.

### 3.2 Nucleus–Nucleus Collisions

The FLUKA implementation of suitable models for heavy ion nuclear interactions has reached an operational stage. At medium/high energy (above a few GeV/n) the DPMJET model is used as described in subsection 3.3. The major task of incorporating heavy ion interactions from a few GeV/n down to the threshold for inelastic collisions is also progressing and promising results have been obtained using a modified version of the RQMD-2.4 code.

### 3.3 The FLUKA - DPMJET Interface

DPMJET-II.53 [23], a Monte Carlo model for sampling h–h, h–A and nucleus–nucleus (A–A) collisions at accelerator and cosmic ray energies ( $E_{lab}$  from 5-10 GeV/n up to  $10^9$ - $10^{11}$  GeV/n) was adapted and interfaced to FLUKA. FLUKA implements DPMJET-II.53 as an event generator to simulate A–A interactions exclusively. DPMJET (as well as the FLUKA high energy h–A generator) is based on the Dual Parton Model in connection with the Glauber formalism. The implementation of DPMJET is also considered a possible, future option to extend the FLUKA energy limits for hadronic simulations in general. Internally, DPMJET uses Glauber impact parameter distributions per projectile–target combination. These are either computed during initialization of the program or can be processed and output in a dedicated run of DPMJET in advance. The computations are CPU intensive for heavier colliding nuclei and it would not be practical to produce the required distributions repeatedly while processing full showers in FLUKA. Therefore, a procedure was devised to efficiently provide pre-computed impact parameter distributions for a complete matrix of projectile–target combinations up to a mass number  $A=246$  over the whole available energy range [24].

FLUKA requires A–A reaction cross sections internally in order to select A–A interactions appropriately. Hence, a complete matrix of A–A reaction cross sections was prepared along with the Glauber impact parameter distributions. Owing to the well established validity of the Glauber formalism, these cross sections can be safely applied down to a projectile kinetic energy  $\approx 1$  GeV/n. DPMJET is called once per A–A interaction. A list of final state particles is returned by DPMJET for transport to FLUKA, as well as up to two excited residual nuclei with their relevant properties. De-

excitation and evaporation of the excited residual nuclei is performed by calling the FLUKA evaporation module.

#### 4. Results and Discussion

The latent tracks are produced when a highly ionizing particle traverses through the CR-39 plastic track detectors. Consequently, damages appear in the polymer bonds due to the energy deposition by the projectile. The nuclear fragments with integral charges are clearly resolved with the measurement of the etch pits on both sides of the CR-39 nuclear track detectors. In principle, the etch-pit areas increase with increasing ion charges.

Measurement of the diameters and length of the etch pits is, therefore, used to estimate the charge of the fragments. The Pb-ions are fully stripped and the detected charges are indicated by arrows in Fig.3. The small peaks to the left of the largest one are due to the fragmented-Pb peaks (lower-charge nuclei). It maps the etch-pit minor axes into incident projectiles of charge  $Z \leq 82$ , fragmented incident projectiles down to  $Z \geq 63$  and pick-up nuclei with  $Z = 83$ . The numbers of unfragmented ions  $Z = 82$ , fragments produced in the charge region  $63 \leq Z \leq 81$  and charge pick-up nuclei  $Z = 83$  have been estimated from the spectrum of cone heights distribution displayed in Fig. 2(a,b).

##### 4.1. Total Charge Changing Cross Sections

The numbers of incident and survived beam ions are determined considering the etched cone lengths distribution of the Pb beam peaks before and after the target. Neglecting the successive fragmentation process in the target, the total charge changing cross sections are determined with the survival fraction of ions using the following formulation of Cecchini et al. [29]

$$\sigma_{\text{tot}} = \frac{A_T}{N_{\text{av}}\rho t} \ln \left[ \frac{N_i}{N_s} \right] \quad (7)$$

where  $A_T$  is the nuclear mass of the target,  $N_i$  and  $N_s$  are the numbers of incident ions before and after the target, respectively;  $\rho$  ( $\text{g}/\text{cm}^3$ ) is the target density;  $t$  (cm) is the thickness of the target and  $N_{\text{Av}}$  is Avogadro number. The measured total charge changing cross sections are shown in Fig. 5. It has been observed that for light target mass region the results of Refs. [4, 5, 6, 26] the cross sections are comparable to cross sections measured in this

work, whereas for the heavy targets our cross sections are significantly larger than those reported [6, 26] at  $\sim 10$ -14 A GeV projectiles and comparable to those observed [4, 5] at similar energy.

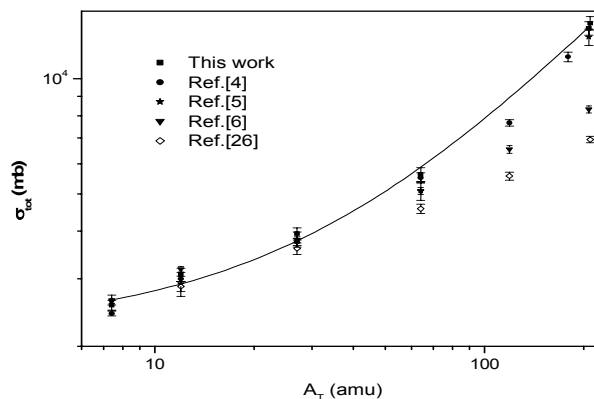


Figure 5. The experimental total charge changing cross sections and the cross sections of reported in Refs. [4, 5] at the similar energy, and Refs. [6, 26] at 10.6 A GeV are shown for comparison. The solid line represents a fit of our experimental cross section to Eqn. 8. The error bars include statistical and systematic uncertainties added in quadrature; systematic uncertainties arise from the measurements of the density and thickness of the targets.

Electromagnetic dissociation plays significant role in the heavy projectile-target collisions at relativistic energy. It can give rise to the process of projectile fragmentation even at impact parameters beyond the range of nuclear forces. Bertulani and Baur [22,23] have derived spectra of virtual photons which strike on the projectile passing by a target nucleus. The photon may be considered representing the time dependent electromagnetic field caused by the target charge  $Z_T$  and seen by the projectile. The projectile nucleus absorbs high energy photons by giant resonances, or by the  $\Delta(1232)$  or higher lying nucleon resonances and decays by emission of one or more nucleons. Possibly, after absorption of a very high energy photon accelerated nucleons penetrate nuclear matter causing fragmentation on their way [22]. The electromagnetic dissociation considerably enhances the total charge changing cross sections particularly in the case of very heavy projectile and target collision [12]. The experimental value of the total charge changing cross sections of Pb projectile fragmentation includes the contribution of nuclear and electromagnetic components of cross section; following the Refs. [6, 7, 29] we fitted the experimental data to Eqn. 8.

$$\sigma_{\text{tot}} = a (A_p^{1/3} + A_T^{1/3} - b)^2 + \alpha Z_T^\delta \quad (8)$$

where  $A_T$  and  $Z_T$  are the atomic mass and atomic number of the target and  $A_p$  is the atomic mass of the projectile. Assuming the values of parameters  $a = 57\text{mb}$  and  $\delta = 1.9$ , we obtained  $b = (0.86 \pm 0.10)$ , and  $\alpha = (1.59 \pm 0.02)$ , with  $\chi^2/\text{d.o.f} = 0.6$ . The solid line in Fig.5 represents this fit.

The total experimental charge changing cross section measured in this work can be described by the Eqn.8, containing both nuclear and electromagnetic components. It has been observed that the nuclear term depends on the atomic mass number  $A_T$  of the target and  $A_p$  of the projectile. The electromagnetic excitation of nuclei in peripheral collisions depends on the beam energy [7]. The main evidence that the process is electromagnetic arises from the observation that the cross sections show charge dependence. The total charge changing cross sections measured are almost comparable with those reported [4,5]. Our measured total charge changing cross sections are significantly higher than those reported in [6, 7, 26] at low energies.

#### 4.2. Semi-Empirical Model Calculation

Total cross sections can also be computed for the comparison with semi empirical models of Bradt and Peters which has an overlap parameter  $b$ , to allow some surface transparency. We have calculated the total reaction cross sections for  $^{207}\text{Pb}$  beam incident on all targets using the Bradt and Peters [20] formula of the form

$$\sigma_{\text{tot}} = \pi r_0^2 (A_p^{1/3} + A_T^{1/3} - b)^2 \quad (9)$$

with best fit parameters for  $r_0 = 1.35 \text{ fm}$  and  $b = 0.83$ .

The probability for projectile nuclei to undergo a charge-changing interaction has been determined from its geometric cross section, as parameterized by Townsend and Wilson [21]

$$\sigma_R = \pi r_0^2 (A_p^{1/3} + A_T^{1/3} - 0.2 - A_p^{-1} - A_T^{-1})^2 \quad (10)$$

where  $r_0$  is an energy independent effective radius,  $r_0 = 1.26 \text{ fm}$ , and  $A_p$  and  $A_T$  are the projectile and target mass numbers, respectively.

Table 2. The nuclear component of the total charge changing cross sections (in mb) of 158 A GeV Pb ions with Bi, Pb, Cu, Al and CR-39 targets calculated using models of Eqns.8, 9 10 have been compared for all targets

Targets	Calculated using Eqn.8	Calculated using Eqn. 9	Calculated using Eqn.10
Bi	6885	6953	6635
Pb	6860	6940	6625
Cu	4674	4726	4612
Al	3699	3743	3692

In the simplest model, the reaction cross sections are assumed to be proportional to the geometrical area of the interacting nuclei ( $\pi R^2$ , where  $R$  is the sum of interacting nuclei radii). Most of the empirical models approximate the total reaction cross section according to Bradt-Peter with

$$\sigma_R = \pi r_0^2 (A_p^{1/3} + A_T^{1/3} - b_0)^2 \quad (11)$$

where  $r_0$  is an energy independent effective radius,  $b_0$  is either an energy independent or energy dependent overlap or transparency parameter, and  $A_p$  and  $A_T$  are the projectile and target mass numbers, respectively. This form of parameterization works nicely for high energies.

The total measured experimental charge changing cross sections are significantly enhanced the semi empirical model calculated cross sections. The excess of total cross section which can be attributed to electromagnetic dissociation processes. It is reported [22] that in relativistic heavy ion fragmentation the process of electromagnetic dissociation plays an important role to increase total cross section. Furthermore, the cross section for EMD, increases almost logarithmically with the energy, exceeds the contribution of nuclear component of cross section of total cross section.

The total charge changing cross section and calculated values of the nuclear and electromagnetic cross sections are shown in fig.6. The uncertainties in the total cross sections are statistical and systematic from the measurement of target thickness and densities. The measured total fragmentation cross sections for all the targets are

compared to FLUKA calculations of total cross sections which are found in good agreement.

The total experimental charge changing cross section measured in this work can be described by the Eqn.8, containing both nuclear and electromagnetic components. It has been observed that the nuclear term depends on the atomic mass number  $A_T$  of the target and  $A_p$  of the projectile. The electromagnetic excitation of nuclei in peripheral collisions depends on the beam energy as reported by [7,27]. The main evidence that the process is electromagnetic arises from the observation that the cross sections demonstrate charge dependence. The total charge changing cross sections measured in the collision of 158A GeV Pb ions are comparable with that reported [4,5] referring similar energies. Our total charge changing cross sections are significantly higher than those reported [6,26] at low energies.

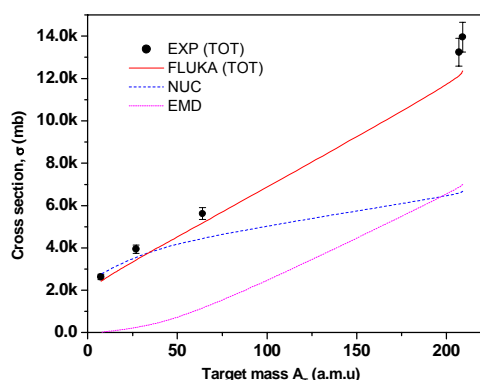


Figure 6 Comparison of total experimental charge changing cross sections with the calculation made with FLUKA model. The calculated nuclear and electromagnetic cross sections of 158A GeV Pb ions as function of target mass are shown.

The dependence on the projectile nuclide, at least for more massive nuclei, can be expressed in terms of neutron content of the projectile. The performance of the detectors established in this experiment not only made it possible to explore charge-changing reactions, but demonstrated the potential of this type of track-etch detector. These measurements done at 158A GeV heavy projectiles collision with heavy targets give insight into both the physics involved and the conditions established in relativistic energy heavy ion collisions. The results from this experiment show the importance of nuclear and electromagnetic

contributions in peripheral collisions involving large impact parameters.

## 5. Conclusions

We have studied fragmentation of 158A GeV Pb projectiles on heavy targets (Bi, Pb, Cu and Al) using CR-39 nuclear track detectors. Based on the data of etched cone heights, the charge resolution of CR-39 detectors has been obtained as  $\sim 0.3e-0.2e$  for the range of detected fragments. A calibration curve for the detector response has also been presented for the heavy fragments with charge  $Z$  from 63 to 82. The charge resolution is determined using the measurement of etched cone heights on a single surface of CR-39 detector.

The total fragmentation charge-changing cross sections for 158 A GeV Pb nuclei interaction with Bi, Pb, Cu and Al targets have been measured using the survival fraction of beam ions in the detectors. The fit of experimental data to the model given in Eqn. 8 has made it possible to estimate the nuclear and electromagnetic components in total fragmentation cross sections. The total experimental fragmentation cross sections for all targets, particularly for heavy targets are found significantly larger in comparison to the calculated using semi empirical models of eqns.10 and 11. However, the measured total fragmentation cross sections are in good agreement with the predictions of the FLUKA model. The enhancement in the total fragmentation charge changing cross sections can be accounted due to the influence of electromagnetic dissociation (EMD) in heavy ion collisions at relativistic energy. It is observed that for the heavy targets the EMD contribution in total fragmentation cross section is almost equal to the contribution of the nuclear cross section, whereas for the light targets the contribution of the nuclear cross section is dominant compared to the contribution of EMD cross sections.

The large values of total fragmentation cross sections in particular measured for heavy targets Bi and Pb can be ascribed due to the influence of electromagnetic dissociation in peripheral collisions. The total fragmentation cross sections observed in these studies are in agreement with similar experimental data in the literature [4,5].

The measured cross section data indicate that CR-39 can be used effectively for studies of the total charge changing cross sections. So, NTDs

provide a considerably good method complementary to active detectors for such studies of nuclear reactions. The total fragmentation cross sections measured for all the targets do not show any energy dependence whereas they depend on the projectile and target masses.

### Acknowledgements

We thank the technical staff of SPS-CERN for the beam exposures. We also acknowledge the contribution and experimental help of Mr. Bashir Ahmad Shad, Physics Division, PINSTECH.

### References

- [1] S. A. Bass, B. Mueller, G. S. F. Stephans, and T. Ullrich (eds.), *Proceedings of the 7th International Conference on Strangeness in Quark Matter SQM2003*, Atlantic Beach, USA, March 12–17 (2003), J. Phys. G: Nucl. Part. Phys. **30**, S1 (2004)
- [2] C.J.Waddington, *Astrophys. J.* **470**, No. 2 (1996) 1218.
- [3] C.J. Waddington, J.R. Cummings, B.S. Nilsen and T.L.Garrard, *Phys. Rev. C* **61**, No. 2 (2000) 024910.
- [4] C. Scheidenberger, et al., *Phys. Rev.C* **70**, No. 1 (2004) 014902.
- [5] H. Dekhissi, G. Giacomelli, M.Giorgini, G. Mandrioli, S. Manzoor, L. Patrizii, V.Popa, P. Serra and V.Togo, *Nucl. Phys. A* **662**, No. 1-2 (2000) 207.
- [6] Y.D. He and P.B. Price, *Z. Phys. A* **348**, No. 2 (1994) 105.
- [7] S.E. Hirzebruch, E. Becker, G. Hüntrup, T. Streibel, E.Winkel and W. Heinrich, *Phys. Rev. C* **51**, No.4 (1995) 2085.
- [8] S. Manzoor, I.E. Qureshi, M.A. Rana, M.I. Shahzad, M. Sajid, H.A. Khan, G. Giacomelli, G. Mandrioli, L.Patrizii, V.Popa, P.Serra and V.Togo, *Nucl. Instrum. and Methods. A* **453**, No. 3 (2000) 525.
- [9] A. Fass`o, A. Ferrari, J. Ranft and P.R. Sala, New Developments in FLUKA Modelling of Hadronic and EM Interactions, in Proceedings of SARE-3, KEK-Tsukuba, H. Hirayama ed., May 7–9 (1997), KEK report Proceedings 97-5, 32 (1997) - A. Fass`o, A. Ferrari, S.Roesler, P.R. Sala, G. Battistoni, F. Cerutti, E.Gadioli, M.V.Garzelli, F. Ballarini, A. Ottolenghi, A.Empl, J. Ranft (2003). The Physics Models of FLUKA: Status and Recent Developments. Computing in High Energy and Nuclear Physics 2003 Conference (CHEP2003), La Jolla, CA, USA, March 24–28.
- [10] A. Fass`o, A. Ferrari, J. Ranft and P.R. Sala, FLUKA: Status and Prospective for Hadronic Applications, in Proceedings of the Monte Carlo 2000 Conference, Lisbon, October 23–26 2000, A. Kling, F. Bar`ao, M. Nakagawa, L. T`avora and P. Vaz eds., Springer-Verlag Berlin, (2001)955.
- [11] A. Ferrari and P.R. Sala, The Physics of High Energy Reactions, in Proceedings of Workshop on Nuclear Reaction Data and Nuclear Reactors Physics, Design and Safety, A. Gandini, and G. Reffo eds., Trieste, Italy, April 1996, **2**, 424 (1998).- A. Ferrari, P.R. Sala, A. Fass`o, J. Ranft, 2005. FLUKA: a multi-particle transport code, CERN-2005-10, INFN/TC-05/11, SLAC-R-773.
- [12] C. Brechtmann and W. Heinrich, *Z. Phys. A* **330** No.4 (1988) 407.
- [13] S. Cecchini, T. Chiarusi, G. Giacomelli, G. Giorgini, A. Kumar, G. Mandrioli, S. Manzoor, A.R. Margiotta, E. Medinaeci, L. Patrizii, V. Popa, I.E. Qureshi, G. Sirri. M. Spurio and V. Togo, *Nucl.Phys.A* **807** No.3-4 (2008) 206
- [14] R.L. Fleischer, P. B. Price and R. M. Walker, *Nuclear Tracks in Solids* (University of California Press)(1975).
- [15] G. Giacomelli, M. Giorgini, G. Mandrioli, S. Manzoor, L. Patrizii, V. Popa, P. Serra, V. Togo and E.C. Vilela, *Nucl. Instr. Meth. A* **411** (1998) 41.
- [16] J.Dreute, W. Heinrich, G. Rusch and B. Wiegel, *Phys. Rev. C* **44** No.3 (1991)1056.
- [17] I.E. Qureshi, M.I. Shahzad, M.T. Javed, S. Manzoor, G. Sher, F. Aleem and H.A. Khan, *Radiat. Meas.* **40**, No.2-6 (2005) 437.
- [18] D.L Henshaw, N.Griffiths, A.L. Landen, Otto and E.V. Benton, *Nucl. Instrum.Methods* **180** No. 1 (1981) 65.
- [19] G.Sher, M.I. Shahzad and M. Hussain, *Radiat. Meas.* **42**, No.10 (2007)1692.

- [20] H.L. Bradt and B. Peters, Phys. Rev. **77** No.1 (1950) 54.
- [21] L.W. Townsend and J.W. Wilson, Radiat. Res. **106**, No. 3 (1986) 283.
- [22] C.A. Bertulani and G. Baur, Phys. Rep. **163** (1988) 299.
- [23] J. Ranft, Phys. Rev. **D51** (1995)64.
- [24] A. Empl, A. Fass`o, A. Ferrari, *et al.*, *Progress and Applications of FLUKA*, Proc. ANS Radiation Protection & Shielding Division 12th Topical Meeting, Santa Fe, New Mexico, USA, April 14–18 (2002), (6 pages, published in electronic format).
- [25] S. Roesler, R. Engel and J. Ranft, *The Monte Carlo Event Generator DPMJET-III*, Proc. Monte Carlo 2000 Conference, Lisbon, October 23–26 (2000), A. Kling, F. Bar`ao, M. Nakagawa, L. T`avora, P. Vaz, eds., Springer-Verlag Berlin (2001)1033.
- [26] L.Y. Geer, J. Kalarman, B.S. Nilsen, C.J. Waddington, W.R. Binns , J.R. Cummings and T.L. Garrard, Phys. Rev. **C52**, No.1 (1995) 334.
- [27] D. Sampsonidis, E. Papanastassiou, M. Zamani, M. Debeauvais, J.C. Adloff, B.A. Kulakov, M.I. Krivopustov and V.S. Butsev Phys. Rev. **C51** (1995) 3304.
- [28] W. R Leo, Techniques for Nuclear and Particles Physics Experiments (Springer-Verlag) (1987) p.26.
- [29] S. Cecchini, H. Dekhissi, V. Garutti, G. Giacomelli, et al., Il Nuovo Cim. **A109** (1996) 1119.